Self-Excited Drop Oscillations in Electrowetting

Jean-Christophe Baret, Michel Decré, Frieder Mugele

Self-excited drop oscillations in electrowetting

Jean-Christophe Baret
Philips Research Laboratories Eindhoven, Prof. Holstlaan 4, 5656AA Eindhoven (NL) [1]
Michel M. J. Decré
Philips Research Laboratories Eindhoven, Prof. Holstlaan 4, 5656AA Eindhoven (NL)
Frieder Mugele
University of Twente, PO Box 217, 7500AE Enschede (NL)

This is the author version of the manuscript published as *Self-excited drop oscillations in electrowetting*, JC Baret et al. Langmuir 2007 (doi.org/10.1021/la062149f)

[1]Present address: ISIS-ULP, 8 allée Gaspard Monge, 67083 Strasbourg, (F)

Abstract

We studied millimeter-size aqueous sessile drops in an ambient oil environment in a classical electrowetting configuration with a wire shaped electrode placed at a variable height above the substrate. Within a certain range of height and above a certain threshold voltage the drop oscillates periodically between two morphologies where it is either attached to the wire or detached from it. We determine the range of control parameters wire height and voltage in which oscillations occur and explain it by a simple capillary model. Furthermore, we analyze the dynamics of the oscillations using high speed video microscopy and numerical fluid dynamics modeling. We develop a one-dimensional harmonic oscillator model that describes the dependence of the drop oscillations on the relevant intrinsic (surface tension, viscosity, density) and extrinsic (wire height, voltage) parameters.

1 Introduction

Micromanipulation of liquid droplets is the basis of digital microfluidic systems in which droplets are the elementary units that carry a biological or chemical content.[1] To be functional, the microfluidic system considered does not only have to provide several elementary handling operations on the unit, like production, actuation, splitting and fusion; it should also be adapted to the particular biochemical constraints of the liquid used, reduce cross-contamination between samples and promote mixing at small scales. Amongst the various ways to actuate liquid at the microscale, electrowetting[2,3] is a particularly promising technique. Its efficiency and versatility has been demonstrated by various groups, not only for functional lab-on-a-chip devices [1,4–9] but also for tunable lenses,[10,11] displays,[12] and optical switches.[13] Despite the large number of applications, modeling of electrowetting has so far mainly been restricted to static situations - except for a few recent contributions. In the present paper we discuss the behavior of drops in a classical electrowetting configuration with a wire shaped electrode held at a variable distance d above the substrate. The electrode is barely immersed into the drop, such that it detaches from the wire upon applying a sufficiently high voltage. After the detachment, no more voltage is applied to the drop and hence it relaxes back towards its shape at zero voltage. Upon doing so, it reattaches to the electrodes whereupon it spreads again, thereby starting a cycle of periodic drop oscillations. The present work is an extension of our previous work on oscillating capillary bridges.[14,15] In a previous communication, we showed that the relaxation of the drop towards its zero voltage shape

can be controlled either electrically if the drop retains a finite charge after the detachment, or purely hydrodynamically if it is discharged during the pinch off from the wire.[16] While the static stability diagram to be described below applies in both cases, for the dynamic part we will focus in the present paper on hydrodynamically controlled oscillations.

The paper is organized as follows: after a brief introduction into the basics of electrowetting at the end of this section, we describe the experimental setup in section II. Subsequently, we present the experimental data and a simple static capillary model to describe the range of stability and instability of both the attached and the detached morphology in the parameter space spanned by the substrate-wire distance d and the applied voltage U (section III). In section IV we analyze the dynamic behavior of the oscillating drops by comparing high speed video microscopy images and numerical (volume-of-fluid) simulations. In the discussion section (V), we map the dynamics of the oscillating drops onto a one-dimensional damped harmonic oscillator. This model turns out to contain all the relevant ingredients to understand the basic physics of the oscillations.

Let us now briefly review the basics of electrowetting. When a drop is deposited on a surface the energies of the various interfaces determine the value of contact angle[17] θ_Y. When a voltage is applied between a conductive liquid and an electrode on a substrate, the solid-liquid interfacial energy decreases quadratically with the applied voltage, as shown by Lippmann in 1875.[18] In recent years, electrowetting on dielectric, a variant of Lippmann's original "electrocapillarity effect" has become *the* standard configuration for electrostatic actuation of sessile drops (see Fig. 1). In this configuration a thin dielectric coating separates the electrode from the liquid and thus prevents electrical currents from flowing. Under these conditions, applying a voltage between the drop and the electrode gives rise to electrostatic charging of the parallel plate capacitor formed by the (perfectly conductive) drop and the electrode on the substrate. The resulting electrostatic energy gain of the system is proportional to the solid-liquid interfacial area. Hence, electrowetting on dielectric - although physically being an electrostatic effect - leads to an *effectively* reduced solid-liquid interfacial energy $\gamma_{sl,eff}(U) = \gamma_{sl,0} - cU^2/2$, where $c = \varepsilon_0\varepsilon_r/T$ is the capacitance per unit area between the drop and the substrate electrode. $\varepsilon_0\varepsilon_r$ is the dielectric permittivity of the insulating layer, T its thickness. As a consequence, the apparent contact angle $\theta(U)$ of the drop depends on both Young's angle and the applied voltage U via the electrowetting equation:[2]

$$\cos\theta = \cos\theta_Y + \frac{c}{2\gamma}U^2 = \cos\theta_Y + \left(\frac{U}{U_L}\right)^2 \qquad (1)$$

where γ the liquid/vapor surface tension. $U_L = c/2\gamma$ is the characteristic voltage scale of the problem. Electrowetting is thus a way to actively control the wettability of a surface by a voltage. In the following we will denote the voltage-dependent contact angle as the apparent contact angle and the contact angle at zero voltage as Young's angle.

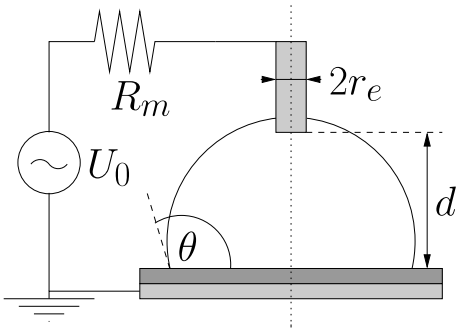

Figure 1: Electrowetting set-up with schematic droplet morphology in the connected state. The drop apparent contact angle (measured by the side-views of the sessile drops) θ is modulated by the rms value of the applied voltage U_0. The distance d is mechanically adjustable. The current is measured via the resistor R_m.

2 Material and Methods

We used a typical electrowetting set-up made of a conductive substrate, an insulating layer, a drop of a conductive liquid (typical volume $V \approx 1\mu l$) and a platinum wire immersed in the drop. The wire (radius $r_e = 50$ or 125 μm) is positioned at a controllable distance d above the substrate. An AC voltage $U = 0$ ... 100 V_{rms} with a frequency $f = 1$...20 kHz is applied between the wire and the solid substrate. The solid substrate is a conductive n^+ arsenic doped silicon wafer (conductivity 1-5 mSm) on top of which a silicon oxide insulating layer has been thermally grown up to a thickness $T = 1.15 \pm 0.15$ μm. An additional hydrophobic layer (OTS monolayer) has been deposited on the surface from the liquid phase using standard protocols.[19] The liquids used are mixtures of water, glycerol and NaCl in various compositions which allows to tune the viscosity η (2 ... 70mPas) and conductivity σ (0.1 ... 10 mS/cm) without significant modification of its surface tension $\gamma \approx 38$ mN/m. The whole set-up is immersed in a silicon oil bath (Wacker silicone oil AK

5, viscosity $\eta = 5$ mPas) in order to (i) prevent evaporation on the time of the experiments, (ii) reduce contact angle hysteresis and (iii) reduce effect of gravity. Young's contact angle θ_Y of the solution under oil, measured using a side view of a sessile drop of water, is 155 $^\circ$ on the OTS layer and about 140 $^\circ$ for glycerol with a few degrees ($<5^\circ$) hysteresis in both cases. The relative density of the liquids in the silicone oil is $\rho = 0.2\text{-}0.3\ 10^3$ kg/m^3. An Ohmic resistor ($R_m = 10$ kΩ) was included in series with the drop (see Fig.1). The current through the circuit is monitored by measuring the voltage across the resistance. The jump of the current amplitude from a zero value in the disconnected state to a non-zero value in the connected state provides an electrical measurement of the drop oscillation frequency. In addition, side-views of the drop are recorded with a high-speed camera (Photron Fastcam ultima 512) at a frame rate of 2000 fps and with an opening time of the shutter in the range 20 - 40 μs.

The apparent contact angle θ was determined from side view images of the

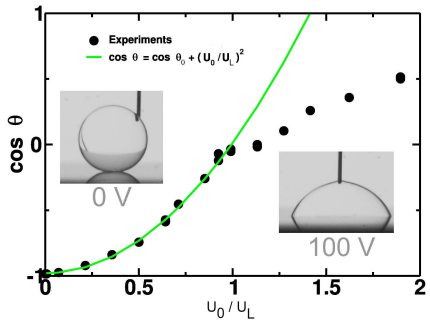

Figure 2: Electrowetting curve for a water drop in oil showing the dependence of the apparent contact angle with the applied voltage. The electrowetting equation 1 holds below 50 V. Here $U_L = 50$ V.

sessile drop using a custom written software. θ decreases with increasing voltage in agreements with eq. 1 up to 50 V [2] (see Fig. 2). The hysteresis between increasing and decreasing voltage is smaller than 5°.

3 Morphology diagram

The experiments were performed as follows. A drop with a radius smaller than the capillary length was deposited on the substrate. The Pt wire was

[2] Above 50 V contact angle saturation set in, as typically observed in electrowetting.[2]

above the drop at zero voltage. There are two possible morphologies for a droplet deposited on a surface: it can be either attached to the wire or detached from it. The stability of both morphologies depends on wire-substrate distance d and on the applied voltage U.[22] We determined the stability limits of both morphologies by varying d and U systematically. The result is shown in Fig. 3, where we rescaled the abscissa and the ordinate by U_L and by $V^{1/3}$, respectively. At large separation (region A), the droplet is always detached from the wire, whereas at small separation (region B), it is always attached. At low voltage, there is a region (C) in which the morphology is history dependent. If region C is entered from above (i.e. from region A), the drop is detached from the wire, whereas upon entering from below (region B) it is attached. In region C both morphologies are thus metastable. The upper boundary of region C, $d_{\max}(U_0)$ (solid line and black circles), represents the stability limit of the attached state, whereas the lower boundary, $d_{\min}$ (dashed line), represents the stability limit of the detached phase. This is the well-known phenomenon of capillary hysteresis. Upon increasing U the width of region C decreases. At the threshold voltage U_T, the stability limits $d_{min}(U)$ and $d_{max}(U)$ cross and continue as smooth continuous functions of U. Placing the wire at a distance d such that $d_{min} < d < d_{max}$ for $U > U_T$ (region D) gives rise to the following situation situation: d is both above the stability limit of the attached morphology and below the stability limit of the detached morphologies. Hence both morphologies are unstable. As a consequence the system oscillates periodically between the attached and the detached state in this region (triangles in Fig. 3).

To characterize this dynamic phase diagram in more detail, we determined the threshold voltage for drop oscillations for various drop volumes V ($V \sim 0.12 \ldots 5.3$ μL) and for two different radii r_e of the electrode (50μm and 125μm). Both increasing V and decreasing r_e were found to reduce U_T (see inset 4).

The raw data could be collapsed onto a master curve by rescaling r_e by $V^{1/3}$, see Fig.4.

To understand this morphological diagram and the behavior of the threshold voltage, we developed a simple capillary model. The stability limit of the detached phase is rather obvious: as soon as

$$d < h(U = 0), \tag{2}$$

where

$$h(\theta(U)) = \left(\frac{3V}{\pi}\right)^{1/3} \frac{1 - \cos\theta(U)}{2 - 3\cos\theta(U) + 3\cos^3\theta(U)}$$

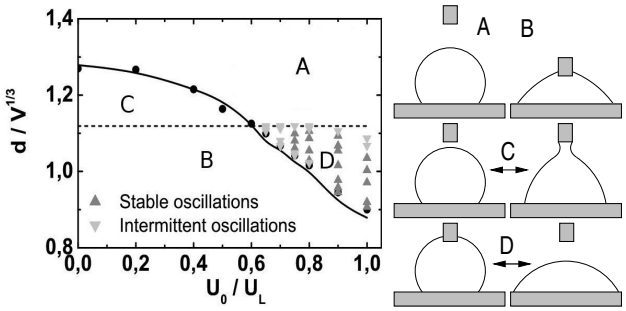

Figure 3: Dynamic phase diagram for a drop of $V \approx 4$ μL with $U_L = 50$ V. In region A, connected states are unstable (the black dots represent the experimental stability limit of the connected morphology.); in region B only connected states are stable; C is the region of capillary hysteresis and D is the oscillation region in which oscillations are stable (triangle up) or unstable (triangle down). The limits of the regions are in agreement with the model (solid line: stability limit of attached morphologies d_{max}; dashed line: height of the drop with Young's angle $h(U = 0)/V^{1/3}$).

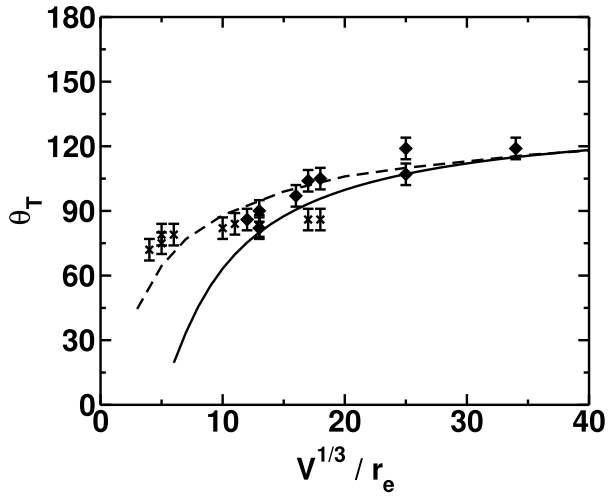

Figure 4: Dependence of the threshold contact angle θ_T with rescaled drop size. Diamonds have been obtained with $r_e = 50$ μm and crosses with $r_e = 125$ μm. The full line corresponds to Eq. 3, the dashed line is obtained by a model based on stability of unduloids.[22]

is the height of the drop at voltage U, the wire touches the drop and thus gets immersed. For drops that are completely discharged after detachment this condition thus gives rise to a voltage-independent horizontal line that depends only on the contact angle if we rescale all lengths by $V^{1/3}$ (see Fig.3). What determines the stability limit of the attached morphology? As long as the drop is sufficiently large compared to the wire, we may regard the attached drop as a spherical cap of (rescaled) height $\tilde{h}(U) = h(U)/V^{1/3}$ with a tiny capillary neck of negligible volume attached to it. The stability limit of the attached morphology is thus determined by the maximum length of that neck. Using Rayleigh's classical argument we expect that the neck becomes unstable when its height is of the order of its circumference $2\pi r_e$ [31] (see e.g. bottom right snapshot of Figure 7). This leads to a maximum height of the electrode:

$$\tilde{d}_{\max}(\theta) = \tilde{h}(\theta) + k\tilde{r}_e \tag{3}$$

where k is a fit parameter, which we expect to be of order 2π. Using the experimental electrowetting curve (Fig.2) to convert the applied voltage into a contact angle, we obtain $k \approx 5$ upon fitting the eq.3 to the experimental data in Fig.3. Obviously, the maximum electrode height decreases with decreasing contact angle, i.e. with increasing voltage. As a consequence, there is - at low voltage - a range of electrode heights for which both morphologies are (meta)stable. At high voltage, however, there is a range of d values where neither morphology is stable. This range of droplet oscillations is determined by the criterion

$$\tilde{d}_{\max}(U) < \tilde{d} < \tilde{h}(0) \tag{4}$$

From this equation it is also clear that the threshold of voltage for drop oscillations is given by $\tilde{d}_{\max}(\theta(U_T)) = \tilde{h}(0)$. The solid line in Fig.4 shows the solution of this equation for U_T (using k=5). It produces good agreement with the experimental data for large volumes, $V^{1/3}/r_e \sim 10$ and larger but fails at smaller volumes. The reason for this failure is that the decomposition of the attached drop into a spherical cap and a capillary neck of negligible volume is no longer justified for small drops. In that range the stability of the exact solutions of the capillary equation, the general axisymmetric surfaces of constant means curvature (Delaunay surfaces) [27] has to be analyzed as described recently.[22] Without any fit parameter it gives rise to the dashed line in Fig.4, which reproduces the experimental results also for small volumes. This analysis also shows that the relevant length scale for the pinch off problem is actually the electrode radius rather that the drop size, which is obviously of no relevance.

4 Dynamics

In the following, we focus on the dynamics of drop oscillations. Assume that we immerse the wire deeply into the drop and set a voltage $U>U_T$. Then we increase d in a quasistatic process to enter the oscillatory region. Upon crossing $d_{max}(U)$, the drop breaks off the electrode. Two different kinds of drop behavior are then observed, depending on the conductivity and the AC frequency of the applied voltage.[16] At low frequency (or at DC voltage) and/or high conductivity, the drop detaches without changing the contact angle substantially (on average). We thus end up with a spherical cap with contact angle $\theta \sim \theta(U)$. On a time scale of many seconds up to minutes (depending on the quality of the insulating layer) θ slowly relaxes back towards θ_Y. At some point the apex of the drop reaches the height d and the drop touches the electrode again. At this moment, the contact angle suddenly drops back to $\theta(U)$, the drop spreads again until it detaches once more from the wire and the entire cycles begins again. This gives rise to highly 'asymmetric' oscillations in which the drop spends most of its time in the detached state and only a short time in the attached one. The explanation of this dynamics is very simple: once the drop is detached from the wire, its contact angle is determined by its charge following

$$\cos\theta_L(q) = \cos\theta_Y + \frac{q^2}{2CA_{sl}\gamma} \tag{5}$$

where $C = cA_{sl}$ is the total capacitance between the drop and the substrate electrode (A_{sl}: solid-liquid interfacial area). For DC voltage, the charge is simply given by $q = Q_{max} = CU$, which means that the contact angle does not change upon detachment of the drop from the electrode. On longer time scales, the drop slowly discharges via unavoidable creep currents, giving rise to the observed slow relaxation of the contact angle and the overall drop shape.

At high AC frequency (and/or at low conductivity), the behavior is completely different. In this regime, the contact angle increases immediately more of less to θ_Y upon detachment from the wire. As a consequence, the drop shape evolves back towards a spherical cap with $\theta = \theta_Y$ on a time scale of order milliseconds rather than seconds to minutes. During this process, it touches the wire again, whereupon the contact angle switches back to $\theta(U)$ and the cycle starts again. This gives rise a very fast drop oscillations with a frequency ranging from ∼10Hz to ∼100Hz, depending on the exact drop size and the viscosity. These fast oscillations are thus much more symmetric with the fraction of time spent in the attached state, t_{on}, and the detached

state, t_{off}, both being of the order of tens of milliseconds. Details, however, still depend on both d and U, as will be discussed below.

From eq.5 it is obvious that the rapid increase in contact angle in the fast oscillatory regime implies that the drop is essentially discharged after the detachment process. We described in detail in a previous publication[16] that such a discharge can indeed take place during the last moments of pinch off of the capillary neck. In that work we showed that the charge in the final state is determined by a balance of three factors: (i) the AC frequency, (ii) the RC-time constant formed by the ohmic resistance of the capillary neck (which diverges algebraically upon pinch off) and the capacitance between the drop and the substrate electrode, and (iii) a characteristic hydrodynamic time scale τ of the capillary pinch off, which depends on the oil-water interfacial tension and the viscosity. All these factors can be combined in a dimensionless parameter $\alpha = 2\pi f(R_0 C t_0^{\mu})^{1/(1+\mu)}$. In this expression $1/2<\mu<3/2$ is the exponent of the neck resistance divergence and $R_0 = 1/\sigma r_e$ is the characteristic resistance of the neck. For $\alpha \ll 1$ the drop charge varies randomly between $\pm Q_{max} = CU$, for $\alpha \gg 1$, however, it goes to zero [3] In the following, we will focus on fast oscillations with $\alpha \gg 1$.

Fig.5 shows the electrical current through the circuit, which displays a non-zero value when the drop is in contact with the electrode during drop oscillations. Fig.5(a) corresponds to parameter values of d and U deep inside oscillatory region.

Oscillations are very periodic and the frequency is well-defined. The absolute frequency depends on both parameters. For instance, for a $\sim$4 μL drop of viscosity 15 mPas frequency of the oscillations is increasing from 26 Hz at 37 V to 42 Hz at 50 V with only a few percent variation when d is varied in the whole range of the oscillating regime. Furthermore, the frequency also depends on the drop size and on the viscosities. However, no significant variations have been observed with the electrical conductivity (within the range that guarantees complete drop discharge upon detachment).

The measurement of the electrical current allows to measure the time spent in the attached state and in the detached state. Variations of d do affect the relative time spent in the attached and in the detached state, respectively. In Fig. 6 we display the fraction of time $\alpha_i = t_i/(t_{on} + t_{off}))$ with i=on, off spent in either state as a function of d. As naturally expected, the time spent in the on (resp. off) state increases (resp. decreases) with decreasing (resp. increasing) d.

Close to the boundary of the oscillatory region the oscillation frequency

[3]For intermediate values of α the charge can adopt a random value between zero and an α-dependent maximum value[16]

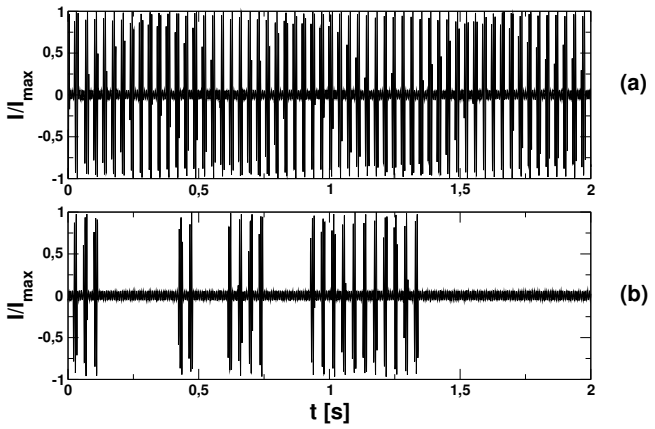

Figure 5: Electrical current indicating the drop / electrode connection. The current is normalized by its maximal value. (a) deep in the oscillating regime ($U = 50$ V, $d = 1.69$ mm) the oscillations are stable. (b) close to boundary ($U = 40$ V, $d = 1.73$ mm), the oscillations are erratic.

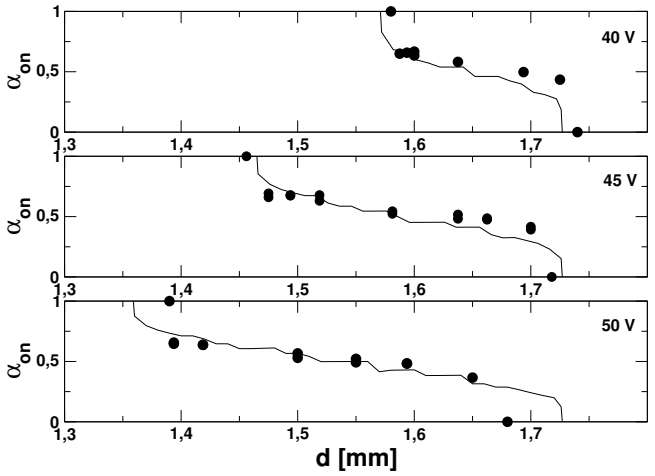

Figure 6: Time spent in the on state as a function of distance for 3 voltages in the oscillating regime. Experimental data (+) and comparison with the model (full line). The parameters of the model are θ =100, 90 and 80 degrees (top to bottom), $\mathcal{Q} = 0.5$, V =3.76 μL, $\theta_Y = 140$ degrees in reasonable agreement with the experimental values.

is not well-defined. Fig. 5(b) shows that the oscillations are rather irregular with periods of slowly relaxing drops (via creep currents; see above) interchanging with periods of fast oscillations.

Apart from the parameters d and U, which control also the morphological diagram in Fig. 3, the oscillation dynamics depend also on the viscosity of the drop and on its volume. Two typical dynamics of oscillations have been observed. For large volumes and small viscosities the drop shape displays large amplitude deformation while for small volumes and large viscosities the drop remains more or less spherical cap shaped. In both cases, the apparent contact angle of the drop is a dynamic advancing contact angle close to the electrowetting angle $\theta(U)$ in the connected state and a receding contact angle close to Young's angle θ_Y in the disconnected state. The switch from $\theta(U)$ to θ_Y and back occurs on time scales much faster than the oscillation period. Examples (snapshots from high speed video clips) of the two types of oscillations are displayed in Fig. 7(a) and 8(a).

In view of the fast switch of the contact angle, we concluded that the oscillation dynamics are in fact completely determined by the hydrodynamic response of the drop to this instantaneous change of the boundary condition. To test this idea, we implemented a numerical simulation scheme of drop oscillations using the volume of fluid (VOF) method with the commercial fluid dynamics package CFD-ACE+ (Fig. 7 (b) and 8 (b)). In the code, the drop dynamics are driven entirely by the switching of the contact angle between the indicated values as the drop either detaches from the wire or reattaches to it [4]. As becomes apparent from the figures, the qualitative features of the dynamics are rather well reproduced - although the absolute oscillation frequency is not perfectly reproduced (see below). Table 1 shows the variation of the times spent in the attached and the detached states, respectively, as well as the oscillation frequencies for a series of parameter values.

These results confirm on a semiquantitative level the validity of the approach taken here. The oscillation dynamics are entirely determined by the hydrodynamic response of the drop to variations of the contact angle. Electric fields do not influence the drop oscillations directly. They enter only indirectly via the induced variation of the contact angle. While the overall drop shapes are correctly reproduced by the numerical calculations, a quantitative comparison of the frequencies shows a slight mismatch, probably caused by the difference of the parameters between experiments and simulations or more fundamentally by the physical description of the contact line motion.

Both the experimental results as well as the numerical calculations show

[4] Numerical methods such as VOF are known to have difficulties in capturing accurately singularities such as during capillary pinch off. However, since the pinch off occurs on a time scale much smaller than the period of the drop oscillation we do not expect such errors to play an important role for the overall dynamics.

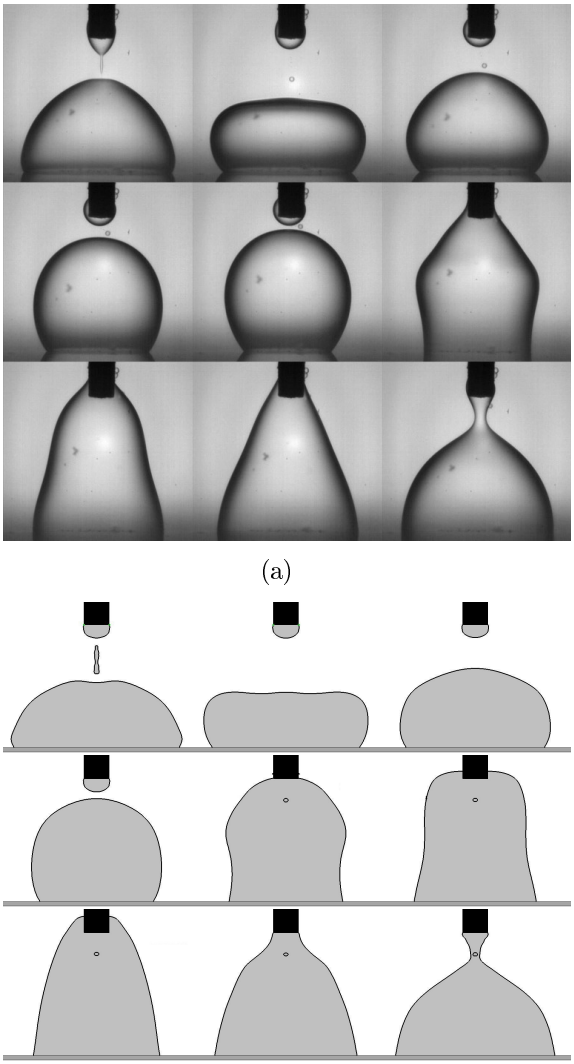

Figure 7: High-speed snapshots of the oscillations of 1 μL aqueous drop in oil and corresponding numerical simulations (VOF, CFD-ACE+ package), inertial regime $\eta \approx 2$ mPas. (a): $d = 1.26$ mm, $F = 72$ Hz, time between two frames 1.5 - 2 ms. (b): numerical calculation $d = 1.21$ mm, $F = 93$ Hz, time between two frames 1.4 ms.

that the oscillation frequency depends strongly on the contact angle. During the oscillations, one should obviously take into account the speed-dependent dynamic contact angle rather than the static value, which we used here. Furthermore, it is to be expected that electric field-induced distortions of the

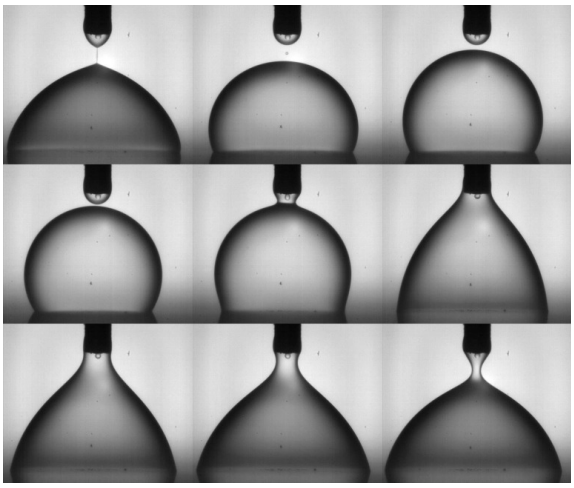

(a)

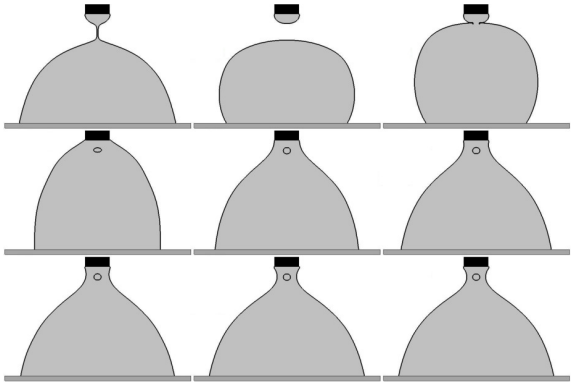

(b)

Figure 8: High-speed snapshots of the oscillations of 1 μL aqueous drop in oil and corresponding numerical simulations (VOF, CFD-ACE+ package), viscous regime $\eta \approx 80$ mPas. (a): $d = 1.10$ mm, $F = 24$ Hz, time between two frames 5 ms.(b) $d = 1.10$ mm, $F = 34$ Hz, time between two frames 3.7 ms

drop surface profile, which are already present in the static situation,[26] or dynamic aspects of the entrapment of thin films of the ambient oil,[20] also affect the drop dynamics. Such effects, however, require additional simulations with more sophisticated numerical tools than currently available to us. Within the scope of the present analysis, we content ourselves with the conclusion that the qualitative aspects of the oscillation dynamics for both low viscosity inertia-dominated drops as well as for viscosity-dominated drops are well reproduced.

		d (mm)					
θ [deg]		0.90	1.00	1.10	1.15	1.17	1.20
50	t_{on} [ms]	40					
	t_{off} [ms]	7					
65	t_{on} [ms]	∞	51	14	13	13	9
	t_{off} [ms]		6	8	9	10	13
75	t_{on} [ms]		∞	25	16	14	
	t_{off} [ms]			8	9	10	
85	t_{on} [ms]			∞		32	
	t_{off} [ms]					10	

Table 1: Numerical simulations results: time in the connected state (t_{on}) or disconnected state (t_{off}).

5 Discussion

By changing the contact angle abruptly between a low and a high value upon breaking the capillary neck or upon reattaching to the electrode, we excite oscillations of the drop. The spectrum of eigenfrequencies of free drops was investigated by Lamb.[21] The evolution of the drop shape suggests that several eigenmodes are excited simultaneously, in particular for the low viscosity case. Rather than analyzing these eigenmodes in detail we will analyse the oscillating drops as a simple damped harmonic oscillator in order to provide a physical understanding of how the oscillation dynamics depend on (i) parameters characterizing the drop (density and size, viscosity, surface tension) and (ii) on the external control parameters d and U.

To perform the mapping, we follow a model similar to the one described by Okumura *et al.*[30] for bouncing drops on superhydrophobic surfaces. The deformations induced by the fast changes of the contact angle are balanced either by viscous dissipation or by inertia or a combination of both. The drop shape is described in radial coordinate by a function $R = R_0 + R_1(\phi, t)$ with R_0 the drop radius at rest (zero voltage), R_1 a time-dependent perturbation and ϕ the angle with respect to the vertical (see Fig. 9).

In order to determine the time-scale of the drop dynamics we consider the Navier-Stokes equation expressing the balance of acceleration by capillary forces and viscous dissipation:

$$\frac{\mathrm{d}u}{\mathrm{d}t} + u\nabla u = \frac{\eta}{\rho}\nabla^2 u - \frac{1}{\rho}\nabla p \tag{6}$$

where the speed $u \sim \mathrm{d}R/\mathrm{d}t$. From a dimensional perspective, we find $u \sim$

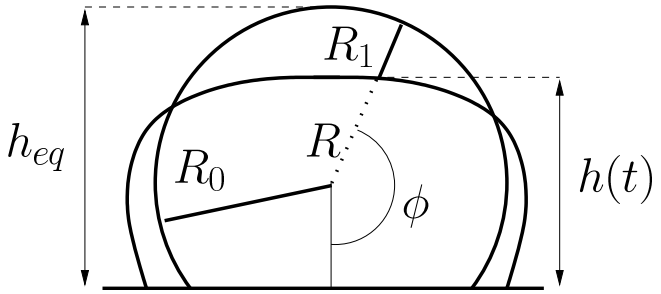

Figure 9: Sketch of the capillary problem considered. The relaxation of the perturbation ϵR_1 is balanced by viscous dissipation or inertia. h is the height of the apex of the drop (see Eq. 8 and 9)

R_1/τ where τ is the time-scale of the motion, $\mathrm{d}u/\mathrm{d}t \sim R_1/\tau^2$ and $u\nabla u \sim R_1^2/(R_0\tau^2)$. Hence the non-linear term $u\nabla u$ can be neglected as long as the amplitude R_1 of the perturbations is smaller than the drop size R_0. p is the capillary pressure linked to the curvature of the interface $\nabla p \sim \gamma/R_0 \cdot R_1/R_0^2$. Therefore Eq. 6 can be rewritten as a damped harmonic oscillator equation for R_1:

$$\ddot{R_1} + \frac{1}{\mathcal{Q}}\dot{R_1} + R_1 = 0 \tag{7}$$

with a dimensionless time $\tilde{t} = t\omega$ where $\omega_0^2 = \gamma/(\rho R_0^3)$ is the eigenfrequency of the undamped system. The dots indicate time derivatives, as usual. (As already noted, we neglect the presence of higher eigenmodes in this analysis.) The quality factor of the oscillator $\mathcal{Q} = (\rho\gamma R_0)^{1/2}/\eta$ is given by the inverse of the Ohnesorge number $Oh = \eta/(\rho\gamma R_0)^{1/2}$. The latter is the characteristic number appearing whenever viscosity, inertia and capillarity compete with each other, as for instance in drop impact problems[23] and capillary breakup.[24] From eq.7 it is thus clear that the dependence of the oscillation dynamics of the drop parameters is represented by the two parameters ω_0 and Oh in this homogeneous equation.

Depending on the value of Oh different regimes are obtained. In the extreme case of inviscid fluids, $Oh \ll 1$ ($\mathcal{Q} \sim \infty$), the system behaves as a spring without damping. The frequency of the oscillations is therefore given by the only remaining time-scale:

$$F_c \sim \omega_0 = \left(\frac{\gamma}{\rho R_0^3}\right)^{1/2}$$

For the drop shown in Fig. 5 we have $Oh \approx 0.01$, i.e. the system behaves as a weakly damped oscillator. This explains the overshoot above the static

height and the other inertia driven deformations of the drop surface.
In the case of an extremely viscous fluid ($Oh \gg 1$), inertia is of minor importance. Keeping only the viscous term the frequency of the oscillations is now given by the relaxation time of the system:

$$F_v \sim \frac{\gamma}{\eta R_0}$$

For the data shown in Fig. 8 we have $Oh \approx 1$. These oscillation thus fall into the intermediate regime inertia, where capillarity and viscous damping are equally important.

While ω_0 and Oh characterize the intrinsic response of the drop, the experimental control parameters d and U will determine the strength and the time-dependence of the external forces, i.e. the inhomogeneities to be added in eq. 7. To understand this aspect it is convenient to rewrite eq. 7 focusing on the dynamics of the drop apex characterized by $h(t)$, i.e. $R(\phi = \pi)$.

$$\ddot{h} + Oh \times \dot{h} + h = h_{eq} \tag{8}$$

where

$$h_{eq} = \begin{cases} h_0 & \text{for } h(t) < h_c \\ h(U) & \text{for } h(t) > d \end{cases} \tag{9}$$

with $h_c = d - kr_e$ is the critical height where the capillary neck breaks (cf. Eq. 3). For $d - kr_e < h(t) < d$, the value of h_{eq} can adopt either value depending on the history, i.e. $h_{eq} = h(U)$ if the drop was previously attached, and $h_{eq} = h_0$ if the drop was previously detached. This explains the role of the external control parameters: the larger U, the larger the difference between h_0 and $h(U)$ and thus the stronger the external driving force acting on the oscillator. d controls the timing when external forces are switched between the two values.

In Fig.10 we display the results of the dynamics of the drop apex for a viscous drop of volume $V = 3.76$ μL with $\mathcal{Q} = 0.5$. The drop is initally connected to the wire placed at $d = 1.5$ mm at t=0. In this case, $h_{eq} = h(U)$ and the drop apex begins to relax exponentially towards this equilibrium value (dashed line in Fig. 10). Upon doing so, the capillary neck breaks at t_1 whereupon the equilibrium values switches to $h_{eq} = h_0$. Hence the drop begins to relax towards this new equilibrium value (dotted and dashed line in Fig. 10) until it reaches $h = d$ at $t = t_2$, whereupon h_{eq} switches back to $h(U)$, etc. The apex height thus oscillates periodically between d and h_c (full line in Fig. 10, as observed experimentally. The time the systems spends in either the attached (t_{on}) or the detached (t_{off}) morphology and thus the

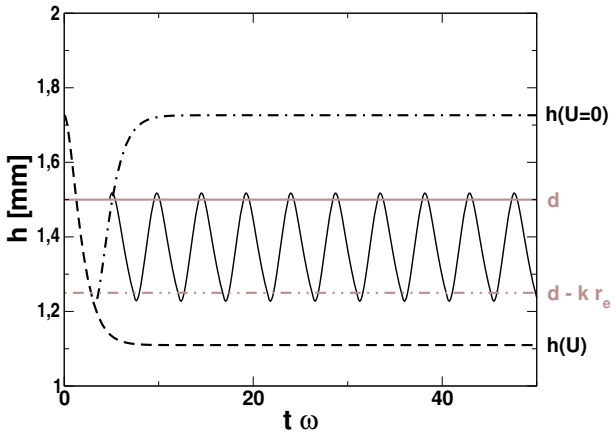

Figure 10: Dynamics of drop apex. Solution of the model for θ_Y =140 degrees, $\theta = 80$ degrees, $\mathcal{Q} = 0.5$, $V = 3.76$ μL. The dashed line corresponds to the spreading without detachment, the dashed-and-dotted line to the relaxation to a drop with Young's contact angle without reattachment and the full line the oscillations. Each time the interface crosses the gray lines, the condition of equilibrium is switched. The over- and under- shoots are results of inertia.

oscillation period is strongly affected by both d and U. For instance it is obvious that t_{on} should increase upon reducing d (and thus h_c). In fact, we expect t_{on} to diverge as h_c approaches $h(U)$. Similarly, t_{off} is expected to increase and diverge as d is increased and approaches h_0. A comparison of the model with the experimental measurements of t_{on} is displayed on Fig. 6 showing that the model predicts correctly the variations of the experimental points. The model however overestimates the drop frequency by a factor of $\sim$2 which might be caused by additional dissipations (at the contact line or in the surrounding fluid) that are not considered here. If we include the effect of inertia into this picture, the main qualitative difference is that we expect the value of $h(t)$ no longer to be confined between d and h_c. Rather, dynamic overshoots and undershoots will occur, as observed in both the experiments and the numerical simulations (see Fig.7). In agreement with the experiments, these overshoots also explain that drop oscillations (once started) can be observed at wire positions $d > h_0$ for low viscosity drops.

The model gives also a qualitative explanation for the irregular burst-like oscillations observed close to the edge of the oscillatory region. In most experiments there is still a small random residual charge charge q on the drop after the detachment, with a maximum value is given by Q_{max}.[16] This

reduces the equilibrium height of the drop from h_0 to $h(q)$, as can be derived from eq.5. If $h_0 < d < h(Q_{max})$ the randomly picked value of q determines whether the drop can reach the wire within the hydrodynamically governed time-scale of the fast oscillations or not. For d just above $h(Q_{max}$, this is the case after most detachment events, but sometimes q is sufficiently close to Q_{max} such that the oscillations are blocked for a certain time.

6 Conclusions

In summary we were able to quantify the geometric and electric conditions required for the generation of self-excited drop oscillations in electrowetting. A simple geometric capillary model was developed to identify the regions within the two-dimensional parameter space $d - U$ where drop oscillations occur, including the threshold voltage U_T. To model the oscillation dynamics, the drop was mapped onto a damped harmonic oscillator in which the intrinsic fluid parameters determine the response of the droplet to an external force that is switched periodically between two values as the drop attaches to the wire and detaches from it. The timing of the external force is set by the external control parameters d and U. From a more general perspective, the success of the modeling presented in this work corroborates two statements that apply to more or less any electrowetting experiment: (i) the characteristic hydrodynamic response times of drops are determined by the balance of three intrinsic fluid dynamic properties of the drops: surface tension, viscosity, and density. The relative importance of these three contributions can be read from the Ohnesorge number $Oh = \eta/(\rho\gamma R_0)^{1/2}$. (ii) variations of the contact angle are instantaneous on the time scale of the typical hydrodynamic response times of the drops. Under usual experimental conditions, there is thus a separation of time scale. As a consequence, the drop dynamics can be modeled by an instantaneous variation of the local contact angle to the voltage applied to the electrode(s) in the system, followed by a purely hydrodynamic response of the liquid on longer times.

We thank Renate Nikopoulos, Udo Krafft and Manfred Hörger for technical assistance. We are also indebted to Ralf Seemann, Stephan Herminghaus and Martin Brinkmann for fruitful discussions and comments on the manuscript. This work was supported by the German Science Foundation within the priority program Wetting and Structure Formation at Interfaces and by the Institute of Mechanics, Process and Control Twente (IMPACT). J.-C. Baret acknowledges support by a Marie Curie Industry Host Fellowship IST-1999-80004.

References

1. Pollack, M. G.; Shenderov, A. D.; Fair, R. B. *Lab on a Chip* **2002,** *2,* 96-101.

2. Mugele, F.; Baret, J.-C. *J. Phys. Cond. Matter* **2005,** *17,* R705-R774.

3. Darhuber, A. A.; Troian, S. M. *Annu. Rev. Fluid Mech.* **2005,** *37,* 425-55.

4. Cho, S. K.; Moon, H.; Kim, C. J. *J. Microelectromechanical systems* **2003,** *12,* 70-80.

5. Srinivasan, V.; Pamula, V. K; Fair, R. B. *Lab Chip* **2004,** *4,* 310-315.

6. Dubois, P.; Marchand, G; Fouillet, Y.; Berthier, J; Douki, T.; Hassine, F; Gmouth, S.; Vaultier, M. *Anal. Chem.* **2006,** *78,* 4909-4917.

7. Wheeler, A. R.; Moon, H; Kim, C. J.; Loo, J. A.; Garrell, R. L. *Anal. Chem* **2004,** *76,* 4833-4838.

8. Yoon, J. Y.; Garrell, R. L. *Anal. Chem* **2003,** *75,* 5097-5102.

9. Paik, P.; Pamula, V. K.; Fair, R. B. *Lab Chip* **2003,** *3,* 253-259.

10. Berge, B.; Peseux, J. *Eur. Phys. J.* **2000,** *E,* 159-163.

11. Hendriks, B.; As, S. K. M. V.; Renders, C.; Tukker, T. *Optical Review* **2005,** *12,* 255-259.

12. Hayes, R. A.; Feenstra, B. J. *Nature* **2003,** *425,* 383-385.

13. Krupenkin, T.; Yang, S.; Mach, P. *Appl. Phys. Lett.* **2003,** *82,* 316-318.

14. Klingner, A.; Herminghaus, S.; Mugele, F. *Appl. Phys. Lett* **2003,** *81,* 4187-4189.

15. Klingner, A.; Buehrle, J.; Mugele, F. *Langmuir* **2004,** *20,* 6770-6777.

16. Baret, J.-C.; Mugele, F. *Phys. Rev. Letters* **2006,** *96,* 106106.

17. Young, T. *Philos. Trans. R. Soc. London* **1805,** *95,* 65-87.

18. Lippmann, M. G. *Ann. Chim. Phys* **1875,** *5,* 494.

19. Sagiv, J. *J. Am. Chem. Soc.* **1980,** *102,*.

20. Staicu, A.; Mugele, F. *Phys. Rev. Letters* **2006,** *97,* 167801.

21. Lamb, H. *Dover Publications; 6th Edn.* **1993,** .

22. Baret, J.-C.; Brinkmann, M. *Phys. Rev. Letters* **2006,** *94,* 146106.

23. Schiaffino, S.; Sonin, A. A. *Phys. Fluids* **1997,** *9,* 3172-3186.

24. Eggers, J. *Rev. Mod. Phys.* **1997,** *69,* 865-929.

25. Berge, B. *C. R. Acad. Sci. III* **1993,** *317,* 157.

26. Buehrle, J.; Herminghaus, S.; Mugele, F. *Phys. Rev. Lett.* **2003,** *91,* 6101.

27. Delaunay, C. *J. math. pures et appliquées* **1841,** *6,* 309-319.

28. Mugele, F.; Klingner, A.; Buehrle, J.; Steinhauser, D.; Herminghaus, S. *J. Phys. Cond. Matter* **2005,** *17,* 559-576.

29. Mugele, F.; Baret, J.-C.; Steinhauser, D. *Appl. Phys. Letters* **2006,** *88,* 204106.

30. Okumura, K.; Chevy, F.; Richard, D.; Quéré, D.; Clanet, C. *Europhys. Lett* **2003,** *62,* 237-243.

31. Rayleigh, L. *Proc. R. Soc. London Ser* **1879,** *A 29,*.